

Recent results on the Higgs boson candidate in the two-photon decay channel at ATLAS

M. SCHWOERER on behalf of the ATLAS COLLABORATION

LAPP, CNRS/IN2p3 and Université de Savoie - Annecy-le-vieux, France

ricevuto il 20 Giugno 2013; approvato l'1 Luglio 2013

Summary. — This paper is intended to give an overview of the results of the ATLAS experiment at the LHC presented in December 2012 for the $H \rightarrow \gamma\gamma$ channel using 4.8fb^{-1} of data taken in 2011 at $\sqrt{s} = 7\text{TeV}$ and 13.0fb^{-1} of data taken in 2012 at $\sqrt{s} = 8\text{TeV}$.

PACS 14.80.Bn – Standard-model Higgs bosons.

1. – Introduction

The 4th of July 2012, both ATLAS and CMS experiments announced the observation of a new boson [1,2]. At that time, the minimum p_0 observed, defined as the probability that the excess seen (or a larger one) is compatible with the background only hypothesis, is 2×10^{-6} at $m_H = 126.5\text{GeV}$. This corresponds to a local significance of 4.5σ . The signal strength μ is defined as the ratio of the signal rate (cross-section) being tested to that predicted by the Standard Model (SM). That is, $\mu = 0$ is the background-only hypothesis and $\mu = 1$ is the SM hypothesis. The best fit value was then $\hat{\mu} = 1.9 \pm 0.5$ at $m_H = 126.5\text{GeV}$.

There are four production modes for a 125.5 GeV Higgs boson at LHC, the main one is the gluon fusion (ggF, 87.4%), then the vector boson fusion (VBF, 7.1%), the vector boson associated production (VH, 4.9%) and the $t\bar{t}$ associated production (ttH, 0.6%) [5]. At LHC peak luminosity in 2012 ($7.7 \times 10^{33}\text{cm}^{-2}\text{s}^{-1}$), about 10 Higgs bosons per minute are expected to be produced. For 1000 Higgs bosons produced, 2 decay in $\gamma\gamma$, mainly through a W loop.

Now that an excess has been observed, it is of first interest to understand if the properties of this particle (contribution of the different production modes, coupling, spin) are compatible with the SM predictions.

2. – Event selection

The ATLAS detector [4] is a multipurpose experiment with a forward-backward symmetric cylindrical geometry and a coverage in solid angle close to 4π . ATLAS uses a right-handed coordinate system with its origin at the nominal interaction point in the centre of the detector, and the z-axis along the beam line. The x-axis points from the interaction point to the centre of the LHC ring, and the y-axis points upwards. Cylindrical coordinates (r, ϕ) are used in the transverse plane, ϕ being the azimuthal angle around the beam line.

We are requiring here events with two isolated photons with a high transverse energy, 40 GeV for the leading photon and 30 GeV for the subleading photon, in the mass range $100 < m_{\gamma\gamma} < 160$ GeV.

Isolation criteria based on the inner tracker and the calorimeter are both applied. The first is the scalar sum of the transverse momenta of all tracks with $p_T > 1$ GeV in a cone of $\Delta R = (\Delta\eta)^2 + (\Delta\phi)^2 < 0.2$ around each photon, and is required to be less than 2.6 GeV. Only tracks originating from the diphoton production vertex are used, and tracks associated to converted photon candidates are excluded. The second variable is the transverse energy sum of positive-energy clusters deposited in the calorimeter around each photon in a cone of $\Delta R = 0.4$, and is required to be less than 6 GeV. The energy sum excludes deposits in the core region which are expected to originate from the photon itself, and corrections for the small estimated energy leakage outside this region are applied. The effects of the underlying event and of additional minimum bias interactions occurring in the same or neighbouring bunch crossings are corrected on an event-by-event basis.

In addition to the isolation and transverse energy cuts, further photon identification requirements are applied on the electromagnetic (EM) shower shape variables [6]. The tight identification is based on 9 variables. The photon efficiency for the tight criteria ranges from 65% to 95% over the E_T range relevant for this analysis.

This selection considerably decreases the reducible background made of γ -jet and jet-jet events where jets fake photons. The rejection factor is about 10^4 . A total of 77430 events of the 8 TeV collisions are selected. The purity in $\gamma\gamma$ events is estimated in a data-driven way [3], based on a sideband method using the two discriminating variables, the isolation and the identification. The background decomposition using this method is shown in fig. 1. The purity is estimated to be about $75^{+3}_{-4}\%$ [7].

3. – Event categorization

The first aim of the categorization was to increase the sensitivity of the search by defining categories with different signal-to-background ratios as well as different invariant mass resolutions (from 1.37 GeV to 2.35 GeV). The baseline analysis uses 9 categories dividing events according to the event properties listed below:

- the η region of the two photons in the calorimeter,
- conversion status of the photon candidates,
- p_{Tt} of the diphoton system.

The p_{Tt} is the diphoton transverse momentum orthogonal to the diphoton thrust axis in the transverse plane [8, 9]. The threshold of 60 GeV, dividing events into categories of low and high diphoton p_{Tt} , is effective due to the discriminating power between gluon

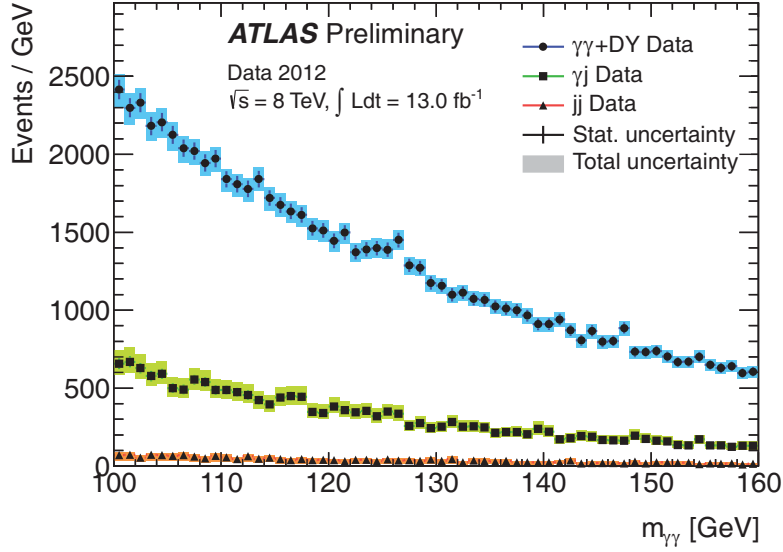


Fig. 1. – 8 TeV diphoton sample composition as a function of the invariant mass. The DY background and signal events are estimated as part of the $\gamma\gamma$ component. The numbers per bin are divided by the bin size [7].

gluon fusion and the other SM Higgs boson production modes. The η and conversion categorizations are independent of the underlying physics. They are motivated by differences in the reconstruction efficiencies and invariant mass resolutions between converted and unconverted photons and the different regions of the detector.

After the discovery, with more statistics, the aim of the categorization was also to improve the uncertainty on the signal strength measurements [7]. The power of the analysis to discriminate between the production modes is enhanced by adding categories that contain different purities of each process.

For VH, two categories reduce the uncertainty on μ_{VH} (see sect. 5). First, a lepton category captures the $W \rightarrow l\nu$ and $Z \rightarrow ll$ decay topologies by requiring an additional lepton in the event. The second VH category is the low mass 2-jets category targeting the event topology of the W and Z hadronic decays. A dijet invariant mass in the range of 60–110 GeV and a pseudorapidity separation between the two jets of less than 3.5 are required. In addition, the p_{Tt} is required to be larger than 60 GeV.

For the VBF, the high-mass two-jets category reduces the uncertainty on μ_{VBF} (see sect. 5). VBF events are characterised by two forward jets with little hadronic activity between the two jets. The high-mass two-jet category collects events containing two jets with invariant mass greater than 400 GeV and a pseudorapidity separation larger than 2.8. In addition, the azimuthal angle difference $\Delta\phi$ between the diphoton and the dijet systems is required to be larger than 2.6.

Events are sequentially sorted into categories in order to avoid any double-counting. In the first step, the VH enriched categories are filled, lepton category first and then the low-mass 2-jets category. The VBF enriched category is the next one and following these VH and VBF enriched categories, the 9 non-overlapping categories based on the conversion status, η region, and p_{Tt} of the diphoton system are filled.

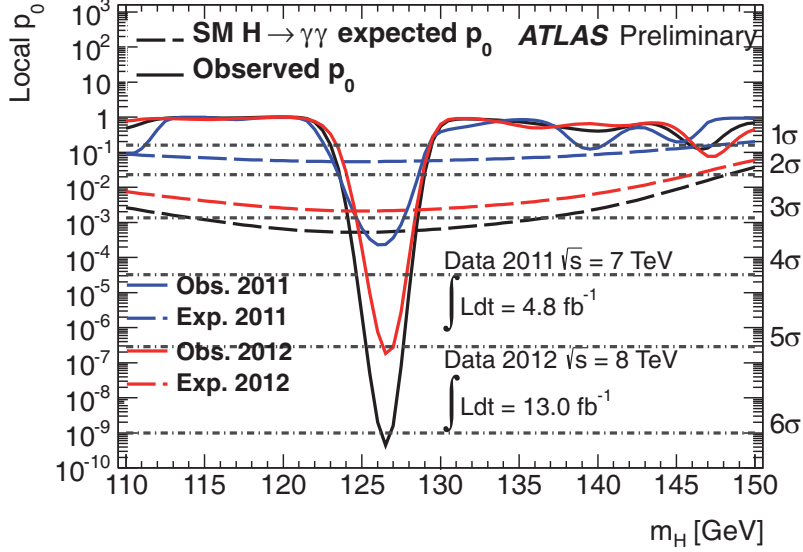


Fig. 2. – Expected and observed local p_0 values for a SM Higgs boson hypothesis as a function of the Higgs boson mass for the combined analysis and for the $\sqrt{s} = 7$ TeV and $\sqrt{s} = 8$ TeV data samples separately [7].

4. – p_0 value and mass of the new particle

The observed local p_0 values as a function of m_H , as well as the expected p_0 values for 4.8 fb^{-1} of data taken in 2011 at $\sqrt{s} = 7$ TeV and 13.0 fb^{-1} of data taken in 2012 at $\sqrt{s} = 8$ TeV, are shown in fig. 2 [7].

The largest local significance is found to be 6.1σ , corresponding to $p_0 = 4.4 \times 10^{-10}$ at $m_H = 126.5$ GeV, where the expected significance is 3.3σ . The diphoton mass scale uncertainty is not included in the evaluation of p_0 , and a modest reduction in the observed significance at a level of 0.1σ is expected if it were accounted for. This confirms the discovery of a new particle in the diphoton channel.

Three main uncertainties enter the mass measurement [3]. The extrapolation from the $Z \rightarrow ee$ energy scale to photons, the material modelling and the presampler energy scale. The electron energy scale extraction from $Z \rightarrow ee$ brings an uncertainty of $\pm 0.3\%$. The uncertainty on the peak position due to material effects when extrapolating the electron energy scale to photons is estimated to introduce an uncertainty of $\pm 0.3\%$. Finally, the uncertainty on the invariant mass peak position due to the uncertainty of the presampler scale amounts to $\pm 0.1\%$.

The best-fit values of m_H and μ , and the corresponding 68% and 95% CL contours are shown in fig. 3. The impact of the systematic uncertainties, and in particular of the diphoton mass scale uncertainty on the precision of the measurement is shown by the modified 68% and 95% CL contours when these systematic uncertainties are removed. At the best-fit $m_H = 126.6$ GeV, $\hat{\mu}$ is found to be $1.80^{+0.42}_{-0.36}$. There is no correlation between mass and μ measurement. The measured signal strength μ is found to be approximately constant over the mass range covered by the systematic uncertainties described before.

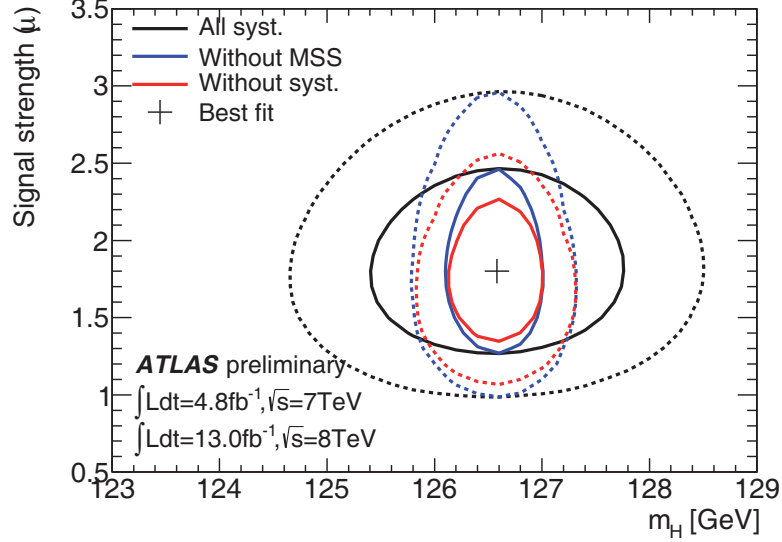


Fig. 3. – The best-fit values of m_H and μ , and their 68% (blue) and 95% (red) CL contours. Results when photon energy scale systematic uncertainties are removed (dashed), and results when all systematic uncertainties are removed (dotted), are also shown [7].

5. – Signal strength per production mode

The consistency or a deviation of the production and decays of the new particle with the expectation for the SM Higgs boson need to be assessed by quantifying the signal yields in different production modes and decay channels. As already mentioned, the categories introduced in the $H \rightarrow \gamma\gamma$ analysis not only improve the sensitivity to the SM Higgs boson signal but also provide some discrimination between the different production modes, given the large variations of the production modes fractions among categories. For instance, the expected contribution of VBF in the low and high p_{T_t} categories is around 4% and 14%, respectively, while it reaches 68% for the VBF category.

For each production mode i , a signal strength factor μ_i defined by $\mu_i = \sigma_i/\sigma_{i,SM}$, where σ is the production cross-section, is introduced [10].

In order to have access to the couplings of the Higgs boson to the top-quark and the vector bosons, the parameters that contribute to each of them — μ_{ggF} and μ_{ttH} in the first case, μ_{VBF} and μ_{VH} in the second — have been grouped together and are multiplied by a common branching ratio factor B/B_{SM} that quantifies the deviation with respect to the SM prediction. This analysis ignores the influence of modified decay couplings which would manifest, for instance, by altering the interferences between the top-quark and W -boson loops. A profile likelihood ratio using $(\mu_{ggH} + \mu_{ttH}, \mu_{VBF} + \mu_{VH})$ as parameters of interest is used as test statistic. The 68% and 95% CL contours are shown in fig. 4.

A simultaneous fit where the VBF and VH production modes are separated is also performed and the best-fit values are given in table I.

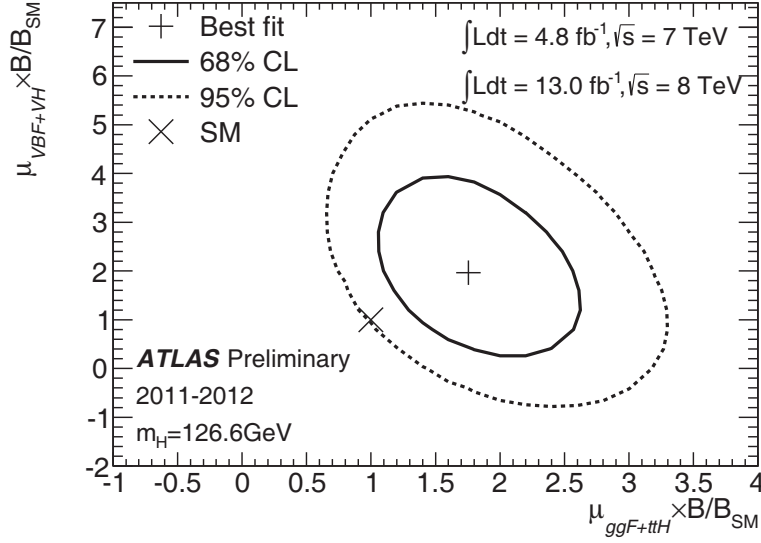


Fig. 4. – The best-fit values (+) of $\mu_{ggF+ttH} \times B/B_{SM}$ and $\mu_{VBF+VH} \times B/B_{SM}$ from a simultaneous fit to the data and their 68% (solid) and 95% (dashed) CL contours. The expectation for a SM Higgs boson is also shown (×) [7].

6. – Study of the spin

The spin-1 hypothesis is strongly disfavored (Landau-Yang theorem) [11]. Two hypotheses for spin (J) and parity (P) are compared: the $J^P = 0^+$ SM Higgs boson and a graviton-like spin-2 state with minimal coupling $J^P = 2_m^+$. This study is based on the distribution of $\cos \theta^*$, where θ^* is the polar angle of the photons with respect to the z -axis in the resonance rest frame (Collins-Soper frame) [12].

The analysis is performed without categorization, on events with diphoton invariant mass in the range [123.8, 128.6] GeV which defines the signal region. The background $|\cos \theta^*|$ distribution is determined from data, with events with $m_{\gamma\gamma}$ within [115, 135] GeV but outside the signal region.

The background-subtracted data distribution is presented in fig. 5 (left), together with the expected signal distributions for the two spin hypotheses taken from MC.

TABLE I. – Best-fit values of signal strength $\times B/B_{SM}$ where B is the branching ratio for $H \rightarrow \gamma\gamma$, for $ggF+ttH$, VBF and VH processes and statistical, systematics and theoretical uncertainties at the best-fit m_H of 126.6 GeV. The theory uncertainty includes the uncertainties on the Higgs boson production cross-section and decay branching ratio [7].

	Value	Stat. error	Syst. error	Theo. error
$\mu_{ggF+ttH} \times B/B_{SM}$	1.8	± 0.4	± 0.2	± 0.2
$\mu_{VBF} \times B/B_{SM}$	2.0	± 1.2	± 0.6	± 0.3
$\mu_{VH} \times B/B_{SM}$	1.9	± 2.5	± 0.6	± 0.4

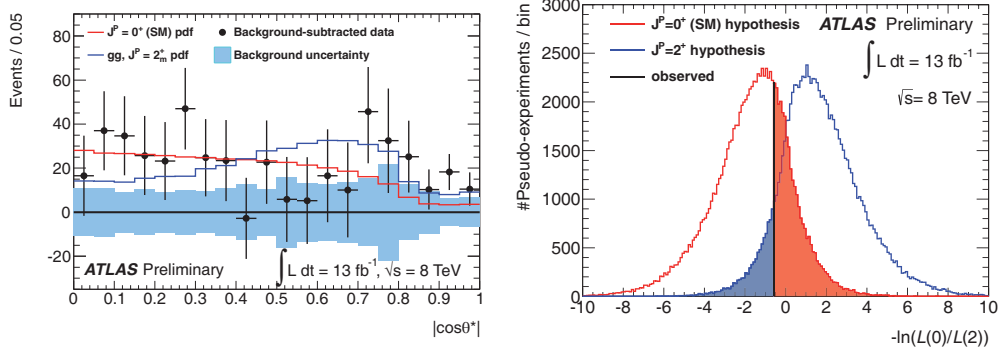


Fig. 5. – Left: background-subtracted data distributions, profiled with a fit where the spin-0/spin-2 ratio (ϵ_0) is free. The fitted value of ϵ_0 is 0.6. The error bars correspond to the data statistical uncertainties only and the blue band shows the background uncertainty before the fit. The two different signal spin pdfs are superimposed. Right: Distribution of q (difference of likelihoods for the fraction of spin-0 $\epsilon_0 = 1$ and $\epsilon_0 = 0$) for the spin 0 (red) and spin 2 (blue) over 100 k pseudo-experiments. The filled histograms illustrate the observed p -values for the two hypotheses [7].

Figure 5 (right) shows the expected distributions of the test statistics q for the spin-0 and spin-2 (produced by gluon fusion) hypotheses; the observed value in data are indicated by the vertical black line.

The expected p -value of a 2_m^+ state signal plus background in pseudo-experiments simulating a SM Higgs boson signal plus background, is $p_{2_m^+} = 3.4\%$. The expected p -value of a SM Higgs boson signal plus background hypothesis, in a pseudo-experiment simulating a 2_m^+ state signal plus background hypothesis, is $p_{0^+} = 3.4\%$. Both expectations correspond to a separation between different spin hypotheses of approximately 1.8σ . The observed q value is -0.59 it corresponds to p -values $p_{2_m^+} = 8.6\%$ (1.4σ) and $p_{0^+} = 29\%$ (0.55σ).

7. – Conclusion

The results presented here are obtained within the search for the SM Higgs boson in the diphoton channel with the ATLAS detector at the LHC using 4.8 fb^{-1} of data taken in 2011 at $\sqrt{s} = 7 \text{ TeV}$ and 13.0 fb^{-1} of data taken in 2012 at $\sqrt{s} = 8 \text{ TeV}$.

An excess of events at around $m_H = 126.5 \text{ GeV}$ is observed with a local significance of 6.1σ . This result confirms the discovery of a new particle reported by both the ATLAS and CMS collaborations and, for the first time, establish the discovery in the diphoton channel alone.

The mass of the boson is measured to be $126.6 \pm 0.3 \text{ (stat)} \pm 0.7 \text{ (syst)} \text{ GeV}$. The signal strength of the new particle decaying to $\gamma\gamma$ final state is $1.80 \pm 0.30 \text{ (stat)}_{-0.15}^{+0.21} \text{ (syst)}_{-0.14}^{+0.20} \text{ (theory)}$ times the SM expectation at $m_H = 126.6 \text{ GeV}$, which is 2.4 standard deviations from the SM expectation. The spin property of the new particle is studied by comparing the data to the SM Higgs boson and specific spin-2 models. The data favours a 0^+ state over the tested spin-2 models.

Results with the full 2012 dataset (20.7 fb^{-1}) have been made public and can be found in [13].

REFERENCES

- [1] ATLAS COLLABORATION, *Phys. Lett. B*, **716** (2012) 1.
- [2] CMS COLLABORATION, *Phys. Lett. B*, **716** (2012) 30.
- [3] ATLAS COLLABORATION, *Observation of an excess of events in the search for the Standard Model Higgs boson in the gamma-gamma channel with the ATLAS detector*, ATLAS-CONF-2012-091, <https://cds.cern.ch/record/1460410> (2012).
- [4] ATLAS COLLABORATION, *JINST*, **3** (2008) S08003.
- [5] LHC CROSS SECTION WORKING GROUP, DITTMAYER S., MARIOTTI C., PASSARINO G. and TANAKA R. (EDS.), *Handbook of LHC Higgs Cross Sections: 2. Differential Distributions*, CERN-2012-002 (CERN, Geneva, 2012).
- [6] ATLAS COLLABORATION, *Expected photon performance in the ATLAS experiment*, ATLAS-PHYS-PUB-2011-007 (2011).
- [7] ATLAS COLLABORATION, *Observation and study of the Higgs boson candidate in the two photon decay channel with the ATLAS detector at the LHC*, ATLAS-CONF-2012-168, <https://cds.cern.ch/record/1499625> (2012).
- [8] VESTERINEN M. and WYATT T. R., *Nucl. Instrum. Methods A*, **602** (2009) 432.
- [9] OPAL COLLABORATION, *Eur. Phys. J. C*, **4** (1998) 47.
- [10] GLEN COWAN, KYLE CRANMER, EILAM GROSS and OFER VITTELS, *Eur. Phys. J. C*, **71** (2011) 1554.
- [11] LANDAU L. and SOPER D. E., *Dokl. Akad. Nauk Ser. Fiz.*, **60** (1948) 207.
- [12] COLLINS J. C. and SOPER D. E., *Phys. Rev. D*, **16** (1977) 2219.
- [13] ATLAS COLLABORATION, *Measurements of the properties of the Higgs-like boson in the two photon decay channel with the ATLAS detector using 25fb^{-1} of proton-proton collision data*, ATLAS-CONF-2013-012, <https://cds.cern.ch/record/1523698> (2013).